

Microscopic and macroscopic aspects of stick-slip motion in granular shearRobert G. Cain,¹ Neil W. Page,^{1,*} and Simon Biggs²¹*Department of Mechanical Engineering, University of Newcastle, Newcastle, NSW, Australia 2308*²*Department of Chemistry, University of Newcastle, Newcastle, NSW, Australia 2308*

(Received 28 December 2000; published 26 June 2001)

An annular shear cell has been used to investigate a number of factors known to influence stick-slip motion in an assembly of near monosized, spherical glass beads. In this paper, both the sample shear stress and volumetric strain were recorded, allowing new insights into the possible mechanics of stick-slip motion in a granular body. Rather than the commonly presented mechanism of sample dilation and fluidization accompanying the slip events, in the material studied here, sample dilation occurred during the preslip deformations of the granular body, while the slip event was accompanied by assembly contraction. Drive velocity and applied normal pressure were both found to influence the magnitude of the stick-slip spikes in a manner analogous to previous studies of stick-slip in assemblies of confined, near-spherical lubricant systems. Finally, atmospheric relative humidity was found to have a marked effect on the magnitude of the stick-slip motion. To investigate this mechanism more fully, the atomic force microscopy was employed to measure the particle-particle interaction forces as a function of atmospheric relative humidity. A water meniscus was found to form under all humidities, from less than 5% to greater than 95%. However, its influence on the adhesive forces varied by an order of magnitude. While most previous studies of stick-slip phenomena have attempted to remove atmospheric humidity as a variable, here we present a useful link between the role of relative humidity on particle-particle interaction forces and the macroscopic response of the granular assembly.

DOI: 10.1103/PhysRevE.64.016413

PACS number(s): 83.80.Fg

I. INTRODUCTION

In recent years, there has been a heightened interest in the stick-slip shear response of assemblies of discrete particles. These studies have been conducted on a range of materials, including granular materials [1,2], boundary lubricants [3–7], and foams [8]. Interestingly, these materials share a number of common traits during stick-slip motion, including the shapes of the stick-slip friction spikes, the existence of a critical velocity for the disappearance of stick-slip motion, and pre- and postcursors to slip. Accordingly, the suggestion has been made that the physical processes occurring in these systems may be quite general, and may even apply on a much grander scale, to earthquakes and the motion of tectonic plates [9]. Indeed, it may happen that the stick-slip response of spherical molecules has more in common with a spherical granular material than with another boundary lubricant made up of chain molecules. For example, Yoshizawa and Israelachvili [4] found that the critical velocity increases with increasing load for OMCTS (octamethylcyclotetrasiloxane, a nonpolar silicone liquid whose quasispherical molecules have a diameter of ~ 0.8 nm), a result also seen here in spherical granular materials (Sec. III), while for chainlike molecules, such as hexadecane (~ 2 nm long and 0.4 nm wide), the critical velocity decreases with increasing load.

In the present paper, some of these similarities are explored in more detail. In studies of the shear properties of lubricant films confined between molecularly smooth mica surfaces, considerable progress has been made mapping the stick-slip response as a function of load, drive velocity, drive

stiffness, and environmental conditions [4–7]. Recently, measurements of this type were also reported with granular materials. Nasuno *et al.* [2] reported measurements of stick-slip motion on granular layers of spherical glass beads sheared between roughened glass plates. They measured the effects of variations in the drive stiffness and velocity, described the creep before and after the slip event in some detail, and measured the instantaneous frictional force during the slip events themselves.

In the current paper, the aim is to investigate the underlying mechanics driving stick-slip motion in systems of discrete media. First the role of drive velocity and applied pressure on the magnitude of the stick-slip friction spikes are examined, allowing a number of comparisons with previous studies. Secondly, the influence of the atmospheric conditions on the stick-slip response are monitored and found to have a significant effect on the magnitude of the stick-slip response. To better understand the origins of this behavior, the atomic force microscope (AFM) colloidal probe technique has been used to measure the particle-particle interaction forces as a function of atmospheric humidity. Finally, by sensitive monitoring of the volumetric strain during stick slip, the relationship between sample dilation and shear strength and the failure properties have been investigated.

A commonly held view is that shear induced “fluidization” and pressure induced “solidification,” accompany stick-slip motion in systems of discrete particles. For example, in computational modeling of stick slip in granular materials, Thomson and Grest report that the material dilates as slip starts, then collapses as the material comes to rest [10]. This is consistent with the mechanism illustrated in Fig. 1. During sticking, the material is “solidlike,” the particles at the interface are closely packed and have a high shear strength. Periodically however, the material dilates and be-

*Author to whom correspondence should be addressed. Email address: npage@mail.newcastle.edu.au

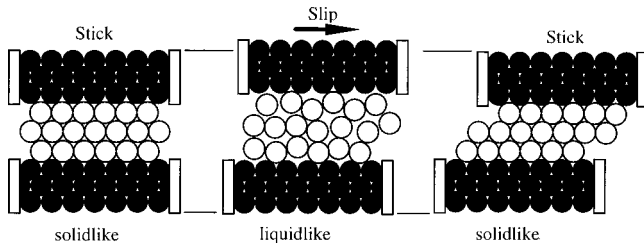


FIG. 1. The transition from static to dynamic states, adapted from Berman, Ducker, and Israelachvili [6]. In the static state, the material in the shear zone, whether a granular material, a confined boundary lubricant, or a foam, is dense and solidlike. To allow slip this material must dilate, becoming more liquidlike.

has like a fluid, allowing the slider to slip. Note, a mechanism of this type (although with variations in terminology) has been used to explain stick slip in both granular materials and boundary lubricants. Interestingly though, the results of Nasuno *et al.* cast some doubt on the details of this mechanism, since in their experiments on sheared granular materials, significant dilation occurs prior to the slip event [2]. However, their measurements of volume change were similar in magnitude to the signal noise level limiting the conclusions that could be drawn from this measurement.

Nasuno *et al.*, also report on the results of microscopic imaging of creep before and after a major slip event [2]. The accumulated precursors were generally found to produce displacements of 1%, those which occurred during a slip event, and most of this occurred immediately before the macroscopic failure of the sample. It has been suggested that these local rearrangement events are a result of breaking force (or stress) chains. It is a well-known property of many granular materials that applied loads are not distributed uniformly. The majority of the load is instead supported by chains of approximately linearly aligned particles. There has been significant progress in characterizing the static [11] and dynamic [12] properties of these stress distributions. Breaking stress chains result in redistributions of the granular packing. Under shear, as stress chains break and reform, small fluctuations in the macroscopic stress occur as the sample creeps; a likely mechanism for the precursor to slip in a granular material. The sensitive measurements of strain and dilation obtained in this paper helps our understanding of these processes.

We note that these irregular displacements before and after a major slip event, have also been reported in studies of thin lubricant films. Demirel and Granick applied oscillatory sliding forces, the amplitudes of which were sufficient to pass from rest to sliding, but small compared to the dimensions of the contact zone. In these experiments, each major slip event was surrounded by erratic minor slip events [7]. These qualitatively similar results suggest the presence of an analogous mechanism to the stress chains of granular materials may also occur in confined lubricant films.

The significance of these results is to demonstrate the complexity of stick-slip motion in systems of discrete particles. One approach is to consider the properties of the individual particles, in an attempt to link these with the macroscopic properties of the bulk material. This is the approach

taken in discrete element modeling of granular materials, in which particles are defined with size, shape, and interaction properties. However, this approach faces a significant hurdle since there is very little experimental data describing the particle-particle interactions, or what links these properties with those of the bulk material. The present paper is distinguished from earlier studies of stick slip in granular materials in that AFM studies of the particle-particle adhesional properties as a function of atmospheric humidity, were performed to complement the macroscopic studies. The AFM approach provides a deeper understanding of surface interactions effects as distinct from the global interactions of assemblies of particles studied in macroscopic experiments. In this way we gain new insight into our understanding of the macroscopic response of the assembly under shear.

II. EXPERIMENT—APPARATUS AND MATERIALS

A. Materials

In the current paper, the effects of atmospheric relative humidity on the particle level adhesive forces were studied using the standardized geometry of a single glass bead on a flat surface, while the bulk shear properties were studied using assemblies of near-monosized, spherical glass beads. The beads were sieved (150–180 μm) near-spherical soda-lime glass (Polysciences, USA). The silica plates used in the AFM, were Suprasil silica, supplied polished to optical smoothness (Groiss, Australia). AFM images of the surfaces revealed that in a $2.5 \times 2.5\text{-}\mu\text{m}$ scan, the standard deviation of the height within the scan area around the mean value was $0.6 \pm 0.2\text{ nm}$. In a $10 \times 10\text{-}\mu\text{m}$ scan, the standard deviation was $1.2 \pm 0.4\text{ nm}$.

The glass surfaces used in the AFM experiments were cleaned in sulphochromic acid then rinsed in Milli-*Q* filtered water. Contact angle measurements on the cleaned surfaces revealed that water formed a wetting film. After 30 min exposure to the atmosphere, the contact angle rose to $25 \pm 5^\circ$. Care was therefore taken to control the environment for the preparation and testing of all samples in the AFM experiments. (Sec. II C). In contrast, there was no provision for controlling the test environment in the annular shear cell. In these experiments the approach taken was to monitor the prevailing temperature and humidity conditions during each experiment. No significant variations in atmospheric conditions were detected through the course of the 30–45 min (including preparation time) of each experiment.

B. Annular shear cell

A Wykham-Farrance annular shear cell was used to measure the response of the granular material under shear. This device was designed by Bromhead primarily for geotechnical research [13], a field in which significant emphasis is placed on the measurement of the sustained yield locus. As the name suggests, this describes the yield behavior of a granular material under large strains. The device, therefore, also lends itself to the study of stick-slip motion in which the unlimited strain allows statistically significant experimental runs to be performed. The experimental apparatus is illustrated in Fig.

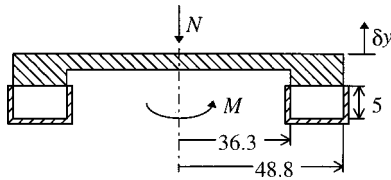


FIG. 2. Schematic of the annular shear cell. A normal load N is applied to the lid and the torque M necessary to restrict the lid from rotating is recorded. Changes in the height of the lid, δy , are also monitored. Dimensions are in millimeters.

2. The sample is poured into the annulus, then scraped level with the edge. The result was a random packing of particles in the test zone. Variations in sample preparation from experiment to experiment did not appear to affect the stick-slip response. A load is applied to the lid, and the torque necessary to restrict the lid from rotating is measured. Any changes in the height of the lid are also monitored using a linear variable differential transformer (LVDT). The noise level of the LVDT as used here was ~ 5 mV while full range (10 V) was amplified to give 2-mm travel. The resolution of the height measurement is therefore ~ 1 μm .

This apparatus allowed us to study the effects of shear velocity, normal load, and atmospheric conditions on stick-slip behavior. However, because it was a constant stiffness device, it could not be used in standard form to investigate the effects of drive stiffness, a feature also known to influence stick-slip behavior [2].

C. Atomic force microscopy

The atomic force microscope (Nanoscope III, Multimode AFM from Digital Instruments) was used to provide a better understanding of the role of atmospheric humidity on the forces of interaction at the points of contact in the granular body. Individual beads were attached with a two part epoxy resin to the end of single beam, etched silicon cantilevers (Digital Instruments, Model TESP). The geometry of the contact region is illustrated in Fig. 3. The experiment involved recording the deflections of the cantilever as a function of relative tip-sample separation as the atmospheric relative humidity was varied. The resulting plots contain information about (i) the thickness of the wetting films on the two interacting surfaces, (ii) the capillary effect of those films, and (iii) the magnitude of the adhesive forces between the surfaces.

The cantilever probes were mounted in a Digital Instrument's fluid cell in a clean laminar flow cupboard and the assembly was then installed in the AFM. High-purity nitrogen (nitrogen $> 99.99\%$, moisture < 12 ppm, oxygen < 10 ppm; BOC gas code #034) was passed through the fluid cell for approximately 30 min prior to an experiment. The relative humidity was then varied by bubbling a proportion of the incoming nitrogen through Milli- Q filtered water. The system was then allowed to equilibrate for 30 min at the given relative humidity. The relative humidity was determined at the outlet of the fluid cell using a Thermo-Hygrometer (Hanna Instruments, HI 91610-C). A slight positive pressure was maintained throughout the experiment to

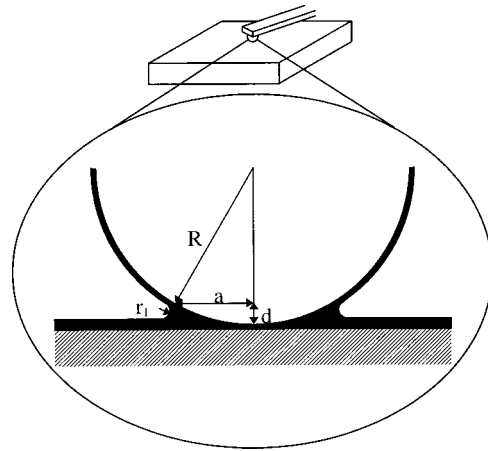


FIG. 3. Schematic diagram of the region of contact in the atomic force microscope showing the parameters used in the discussion. R is the radius of the bead, a is the radius of the area of the meniscus in contact with the bead, r_1 is the concave radius of the meniscus, and d is the height of the meniscus relative to the end of the bead.

ensure no ingress of atmospheric air. Experiments were conducted in an air-conditioned room and the temperature did not vary significantly over the course of the testing program.

III. RESULTS

A. Factors influencing stick-slip motion

1. Velocity

Figure 4 shows the results (shear stress versus drive displacement) of two annular shear cell experiments conducted under the same applied load and with identical atmospheric conditions. The difference in these experiments was the drive velocity; in the first experiment it was 250 $\mu\text{m s}^{-1}$ and in the second experiment it was 2 $\mu\text{m s}^{-1}$. The shear response of the first experiment was essentially steady, while the second experiment showed significant stick-slip motion, indicating a drive velocity dependence of the shear response. The average

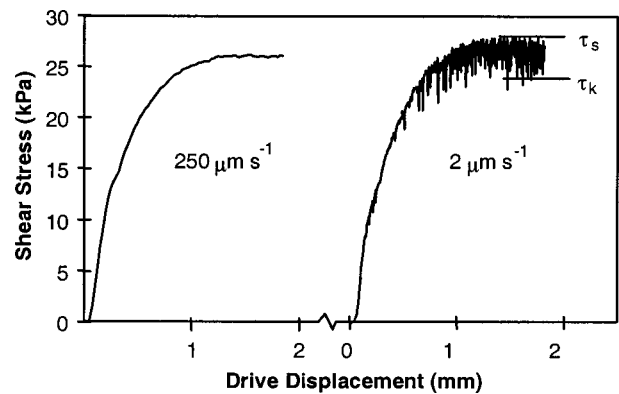


FIG. 4. The shear stress during stick-slip motion plotted against drive displacement for portions of two shear experiments. In the first test, at 250 $\mu\text{m s}^{-1}$, there is no stick-slip during shear, while there is in the second test at 2 $\mu\text{m s}^{-1}$. The two tests were done in identical atmospheric conditions, and the applied normal pressure in both tests was 62 kPa.

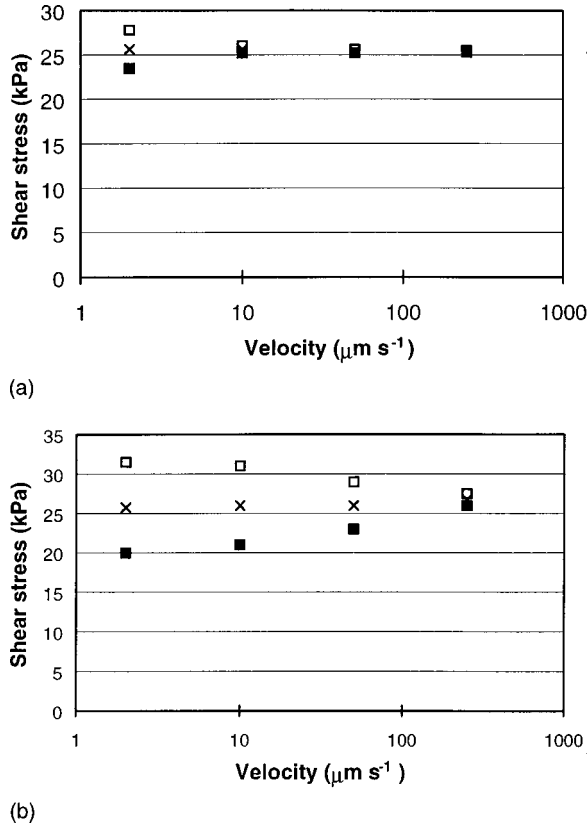


FIG. 5. Maximum (open squares) and minimum (closed squares) shear stresses during stick-slip motion versus drive velocity for testing in two atmospheric conditions. These results are analogous to those of Berman, Ducker, and Israelachvili who investigated the shear behavior of OMCTS confined between mica surfaces (Sec. I) [5]. They also illustrate the strong dependence on atmospheric conditions of the peak shear strengths during stick-slip motion. The temperature and relative humidity were in (a) $23 \pm 1^{\circ}$ and $23 \pm 4\%$, and in (b) $28 \pm 1^{\circ}$ and $38 \pm 4\%$. The crosses are the average of the maximum and minimum shear stresses. The applied normal pressure during all tests was 62 kPa.

maximum and minimum shear stresses, τ_s and τ_k , of the stick-slip response, are also shown in Fig. 4. In Fig. 5, τ_s and τ_k are plotted against the drive velocity for two different atmospheric conditions. (The role of atmospheric conditions will be discussed shortly; for the moment we are interested only in the effects of variations in the drive velocity.) As the drive velocity was increased, the amplitude of the variations in the shear stress decrease until stick-slip motion stops altogether. The velocity at which this occurs is known as the critical velocity, V_c [5].

The average of the maximum and minimum shear stresses, $(\tau_s + \tau_k)/2$, as a function of drive velocity are also shown in Fig. 5. For the range of drive velocities investigated, these were found to remain relatively constant. The shape of these profiles, and the constant value of the average shear stress is analogous to the results reported by Berman, Ducker, and Israelachvili, who investigated the shear behavior of OMCTS confined between mica surfaces (Sec. I) [5]. Berman, Ducker, and Israelachvili suggest that the average of the peak shear stresses is an approximation of the true

kinetic shear strength, i.e., the shear strength at the interface during slip. Furthermore, for a wide range of drive velocities, this material property is constant.

However, Nasuno *et al.* were able to determine the instantaneous shear stress at the interface during the slip event [2]. They found that it was, in fact, a multivalued function of the slider velocity, depending on the acceleration as well as the instantaneous velocity. By contrast, the “true kinetic shear strength” to which Berman, Ducker, and Israelachvili refer, and with which we see parallels in the current paper, is an *average* kinetic interface strength.

2. Atmospheric conditions

In earlier studies of stick-slip motion in granular material, the effects of variations in the atmospheric conditions have been removed by performing experiments in a controlled environment. Without this precaution, significant variations were found to occur from run to run [1,2]. In the present paper, we have taken an alternative approach; in order to investigate the role of adsorbed moisture in the stick-slip mechanism, the atmosphere was monitored rather than controlled.

The two sets of data shown in Fig. 5 also give an indication of the role of atmospheric humidity on the shear response of the material studied here. In Fig. 5(a), the temperature and relative humidity were $23 \pm 1^{\circ}\text{C}$ and $23 \pm 4\%$, while in Fig. 5(b) they were $28 \pm 1^{\circ}\text{C}$ and $38 \pm 4\%$. In Fig. 5(a), the critical velocity is around $100 \mu\text{m s}^{-1}$, while in Fig. 5(b) it has increased to above the range of the experiments, to approximately $1000 \mu\text{m s}^{-1}$. These results are typical of the experiments conducted here. Over the range of atmospheric humidities recorded (which varied between 20% and 55%) any testing below the critical velocity gave larger amplitude stick-slip motion with higher atmospheric relative humidity. These results give an indication of the relationship between stick-slip amplitude and atmospheric conditions, although more testing is required to map the response outside this range of relative humidities, and also to further investigate effects of testing machine stiffness and inertia on these results.

Interestingly, the change in atmospheric conditions from Fig. 5(a) to Fig. 5(b) alters the amplitude of the stick-slip response, but not the average of the peak shear stresses. This indicates that films arising from adsorbed water on the surface of the particles (which is a function of both the temperature and the relative humidity) change only certain aspects of the assembly strength. That is, the assembly property that determines the amplitude of the stick-slip motion, is altered, although not that which determines the average kinetic shear strength.

3. Applied load

The load applied during shear is known to affect the amplitude of stick-slip motion [2]. Figure 6 shows the maximum and minimum shear stresses recorded at a range of applied loads for a given atmospheric condition. As the applied load increases, the amplitude of the stick-slip motion also increases. In Sec. I, we noted that the critical stick-slip

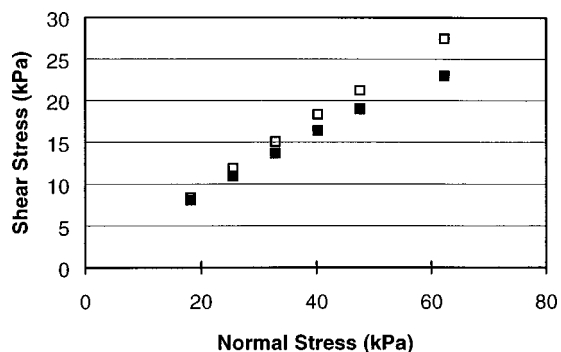


FIG. 6. The average maximum shear stress (open squares) and the corresponding minimum shear stresses (closed squares) during stick-slip motion at a range of applied loads. Each point is the average of two tests. The temperature and relative humidity were 24° and 35%.

velocity increases with load for spherical molecules but not chain molecules [4]. As expected, the results presented here for spherical granular materials resemble those of the spherical molecules. Whether a flexible, chainlike granular material would respond to shear in a fashion similar to the chainlike molecules of Yoshizawa and Israelachvili remains to be investigated.

B. Volumetric strain

An advantage the annular shear cell possesses over other techniques for studying stick-slip motion in granular materials, is the ease with which sample volume changes may be measured. It is known that sample dilation and contraction play a significant role during stick slip. In this section, this process is examined in detail.

In Fig. 7, the variations in the measured shear stress and

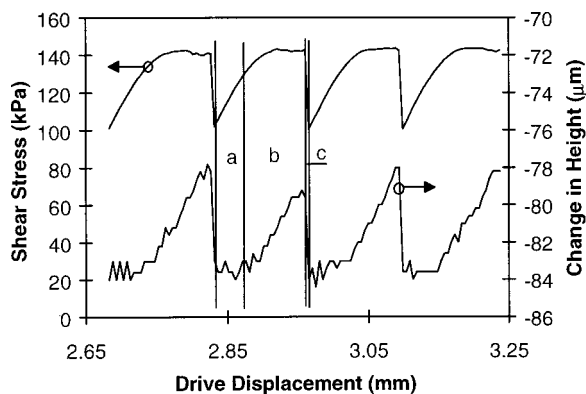


FIG. 7. A portion of an experiment in which the assembly displayed large amplitude stick-slip motion. The shear stress (upper trace, corresponding to the axis on the left) and the change in height (lower trace, corresponding to the axis on the right) are plotted against the drive displacement. Note that the result shown is just 0.6 mm of travel, recorded after the sample had already sheared 2.65 mm. At this point, the material has undergone consolidation of more than $78 \mu\text{m}$, and the sample is varying in height by approximately $6 \mu\text{m}$ with each stick-slip cycle. The drive velocity was $50 \mu\text{m s}^{-1}$, and the applied pressure was 298 kPa. The significance of the lettering is explained in the text.

the changes in the sample height are plotted for “large amplitude” stick-slip motion. This result was recorded for a constant drive velocity of $50 \mu\text{m s}^{-1}$ and an applied pressure of 298 kPa. In any one stick-slip cycle, three stages can be identified, as shown in Fig. 7:

(a) An initial, approximately linear increase in the shear stress occurs as the sample resists all movement, both vertical and horizontal. This is similar to the “sticking” phase illustrated in Fig. 1.

(b) The sample creeps as the shear zone dilates. Note, creep is defined here as any shear strain in the sample other than that of the macroscopic slip event.

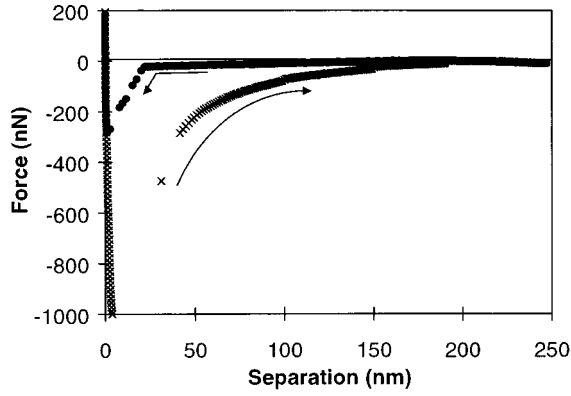
(c) Eventually, the material dilates (and weakens) to such an extent that it can no longer resist the shear stress and the sample slips. The shear stress and sample height return to their original values.

This result is significantly different to previously published descriptions of the stick-slip process. Rather than a simple transition between “solidlike” and “liquidlike,” a significant proportion of the process is taken up in a transition state, in which creep occurs both horizontally and vertically. That is, dilation does not accompany the slip event in a transition to a “liquidlike” state. Rather, dilation occurs with creep as the sample weakens under strain.

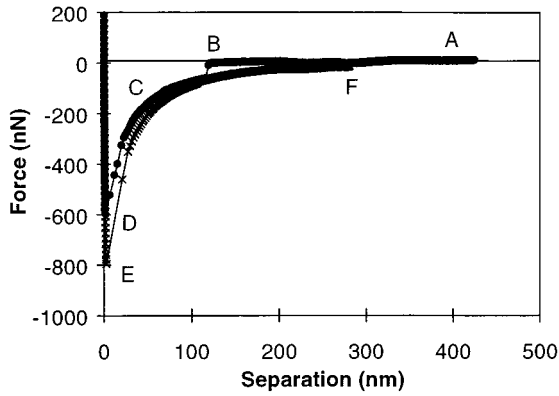
The creep that occurs in a sample before and after a slip event, has been well documented. Nasuno *et al.* report imaging the microslip events in granular materials [2], Demirel and Granick report a similar phenomenon occurring in sheared lubricant films [7], and parallels to the precursors of earthquakes have also been drawn [9]. A mechanism for this process has also been suggested: they are thought to be the result of stress-chain failure [2]. If this explanation were correct, there should be a simple relationship between stress-chain strength and stick-slip amplitude. To this end, in the following section an AFM study of particle interaction strength as a function of atmospheric conditions is described. This comparison is therefore based on the reasonable assumption that granular stress-chain strength is a function of the interparticle forces maintaining contact between the particles.

C. Atomic force microscopy

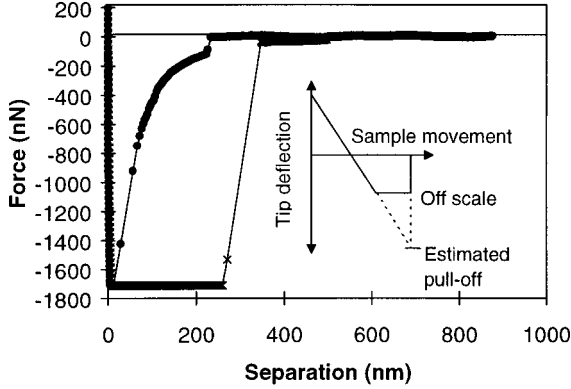
Figure 8 shows the force acting on the cantilever probe as the sample surface approaches, comes in contact with, and then recedes from the bead for interactions at 14%, 30%, and $>95\%$ relative humidity. Referring to the lettering in Fig. 8(b) (recorded at 30% relative humidity) there is no detectable force on the cantilever (A) until contact is made between the liquid films (B). When this occurs, the resulting meniscus leads to a sudden attractive force. The separation at which this occurs is the combined thickness of the films on the two surfaces. At 14% relative humidity, this interaction (if present) is too small to distinguish. However, at 30% and $>95\%$ relative humidity, the liquid films are sufficiently large to result in attractive jumps of 60 and 120 nN, at separations of 120 and 230 nm, respectively. This is a typical result: as the atmospheric relative humidity increased, the



(a)



(b)



(c)

FIG. 8. Force separation curves recorded at (a) 14% relative humidity, (b) 30% relative humidity, and (c) greater than 95% relative humidity. The solid circles are data points recorded as the surfaces are brought into contact and the crosses are those recorded as they are separated. Arrows also indicate the direction of travel in (a). The lettering in (b) is described in the text. The schematic in (c) indicates the method used to determine the pull-off force in cases where the trace went off scale.

thickness of the water films on the two surfaces and the magnitude of the initial jump-in also increased.

Mate *et al.* found that for an AFM tip interacting with deposited liquid polymer films, the jump-in force could be approximated as the Laplace pressure acting over the area of the meniscus [14]. The Laplace pressure for a meniscus between a sphere and a smooth surface is [15]

$$P = \left(\frac{1}{r_1} + \frac{1}{r_2} \right) \gamma_L \approx \frac{\gamma_L}{r_1} \quad (\text{since } r_2 \gg r_1), \quad (1)$$

where r_1 and r_2 are the concave and convex radii of the meniscus, respectively, and γ_L is the surface tension of water ($=72 \text{ mN m}^{-1}$). Using the parameters defined in Fig. 3, this pressure acts over an area $\pi a^2 \approx 2\pi R d$. For $d \ll R$, $d \approx 2r_1 \cos \theta$, where θ is the contact angle between the surface and a droplet of water [15]. Hence, the Laplace pressure contributes an adhesive force

$$F = 4\pi R \gamma_L \cos \theta. \quad (2)$$

In the present system, if we use as an example the largest jump-in force, $F = 120 \text{ nN}$ from Fig. 8(b), and wetting angle $\theta = 0^\circ$, Eq. (2) gives a radius for the bead of 133 nm . This is two orders of magnitude smaller than the bead radius of $15.5 \mu\text{m}$. As will be discussed below, it is not until the surfaces are pulled apart that forces of the order predicted by Eq. (2) are encountered.

Returning to Fig. 8, after jump-in the net force on the bead increases (C) primarily as a result of the Laplace pressure. Other forces including van der Waals, electrostatic, solvation, and hydrodynamic forces [16] also act on the bead. However, the analysis of this region of the force-separation curve is beyond the scope of the current discussion. Eventually, solid contact is made between the sample and the bead (D) and the force quickly becomes positive (AFM cantilever forced up) as the two surfaces are pushed hard against one another.

On sample retraction, the solid surfaces do not separate until a certain ‘‘pull-off’’ force has been applied (E). In Fig. 8(c), this load is beyond the limits of the detection system. However, as the inset in Fig. 8(c) illustrates, an approximate pull-off force can be determined.

Following solid-solid separation, the force-separation characteristics also vary with relative humidity. At or below $\sim 30\%$ relative humidity, the forces on the tip slowly decrease as the sample is retracted until the meniscus breaks at a separation significantly greater than the original combined water film thickness (F). However, at or above $\sim 70\%$ relative humidity, separation is a two-step process. Initially, there is a sudden jump out of solid-solid contact, followed by stretching and final breakage of the meniscus.

In Fig. 9, pull-off forces are plotted as a function of humidity. At or below 30% relative humidity, the pull-off forces were approximately independent of variations in relative humidity, varying from 510 to 1290 nN with an average of 860 nN. At or above $\sim 70\%$ relative humidity, the pull-off forces were again approximately independent of variations in relative humidity, varying now from 3940 to 7080 nN with an average of 5590 nN. Substituting this value into Eq. (2) gives a radius of $6.2 \mu\text{m}$, two and a half times smaller than the bead used in the experiments. However, this is not an unusual result. For a number of reasons, including surface contamination and roughness, and the possibility that the bead slips or rolls as the contact is broken, pull-off forces measured with the AFM are invariably smaller than theory

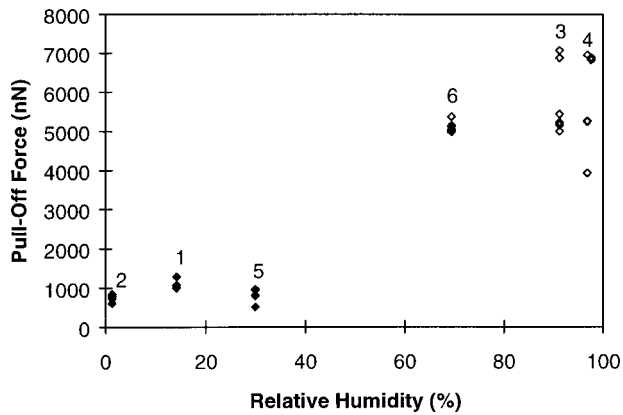


FIG. 9. Variations in pull-off force with relative humidity. At or below 30%, the pull-off force remains relative constant at around 860 nN, while at or above 69%, the pull-off force again remains relative constant, but with an average of 5590 nN. The numbers indicate the order in which the experiments were done, and indicate that there was no history effect in the transition from the low pull-off to the high pull-off regime.

suggests [17]. Of more significance to the current study is the result that the pull-off force increases by an order of magnitude with relative humidity.

IV. DISCUSSION

The measurements of volume change reported here allow new insights into the role of sample dilation and contraction during stick-slip motion. Rather than dilation accompanying the onset of slip, with a transition to a liquidlike state, it occurs with sample creep prior to the slip event. During this process, the assembly gradually weakens until failure finally occurs. Therefore, rather than a simple transition from solid-like to liquidlike, there are in fact three stages to the stick-slip cycles reported here. A more appropriate description of the process may be to consider the elastic loading, plastic creep, and brittle failure of the assembly.

During elastic loading, interparticle relative movement is minimal. Instead, most of the drive displacement is taken up in elastic loading of the drive and the granular assembly. As this progresses, stress chains will form and strengthen. However at some point, the assembly begins to creep, and as it does so, it dilates. Conceptually, this process may involve stress chains rotating into an orientation more aligned with the normal stress. This transition point and the duration of this stage will therefore be functions of the strength of the particle-particle interactions. From the AFM results, we have

seen that there is an order of magnitude increase in the strength of particle-particle adhesion in the region $\sim 30\%$ to $\sim 70\%$ relative humidity, corresponding reasonably well to the humidities at which the shear cell experiments were conducted. Hence the result that even quite small variations in atmospheric relative humidity had a dramatic effect on the magnitude of the stick-slip response, is not unexpected.

Finally, the assembly dilates and weakens to such an extent that the shearing force can no longer be supported. The extent of the resulting failure is then a function of the energy absorbed by the assembly. The failure is largest at low velocities and in humid environments.

V. CONCLUSIONS

Stick-slip motion in a granular material was studied using an annular shear cell in which both the shear stress and the volumetric strain were recorded simultaneously. The stick-slip process could be broken down into three stages: (1) an elastic loading stage, (2) a plastic strain stage, and (3) macroscopic failure. Rather than dilation accompanying failure and a transition to a liquidlike state, the granular material studied here dilated during the plastic strain stage. It was not until the material had weakened considerably that failure occurred.

In the current paper, the effect of changes in atmospheric humidity were also recorded. It was found that an increase in relative humidity resulted in an increase in the magnitude of the stick-slip response. The AFM colloidal probe technique was employed to investigate variations in the strength of the particle-particle interactions as a function of atmospheric relative humidity. It was found that the adhesion increased by an order of magnitude as the relative humidity was increased. This result fits the conceptual model that it is the strength of the load carrying stress chains within the granular assembly that determines the magnitude of the peak-to-peak stress fluctuations during stick slip. Increasing the relative humidity increases the adhesion between the particles, increasing the strength of the stress chains, and hence the stress required to cause a macroscopic slip event. However, this strengthening appears to plateau at relative humidities of greater than about 70%.

ACKNOWLEDGMENTS

This research was supported by the Australian Research Council through its individual research grants scheme, the Center for Bulk Solids and Particulate Technologies and the Center for Multiphase Processes.

- [1] S. Nasuno, A. Kudrolli, and J. P. Gollub, *Phys. Rev. Lett.* **79**, 949 (1997).
- [2] S. Nasuno, A. Kudrolli, A. Bak, and J. P. Gollub, *Phys. Rev. E* **58**, 2161 (1998).
- [3] M. L. Gee, P. M. McGuiggan, and J. N. Israelachvili, *J. Chem. Phys.* **93**, 1895 (1990).

- [4] H. Yoshizawa and J. Israelachvili, *J. Phys. Chem.* **97**, 11 300 (1993).
- [5] A. D. Berman, W. A. Ducker, and J. N. Israelachvili, in *Physics of Sliding Friction* (Kluwer Academic, Dordrecht, 1996), p. 51.
- [6] A. D. Berman, W. A. Ducker, and J. N. Israelachvili, *Lang-*

- muir **12**, 4559 (1996).
- [7] A. L. Demirel and S. Granick, Phys. Rev. Lett. **77**, 4330 (1996).
- [8] A. D. Gopal and D. J. Durian, Phys. Rev. Lett. **75**, 2610 (1995).
- [9] G. B. Lubkin, Phys. Today **50**, 17 (1997).
- [10] P. A. Thompson and G. S. Grest, Phys. Rev. Lett. **67**, 1751 (1991).
- [11] C.-h. Liu, S. R. Nagel, D. A. Schecter, S. N. Coppersmith, S. Majumdar, O. Narayan, and T. A. Witten, Science **269**, 513 (1995).
- [12] B. Miller, C. O'Hern, and R. P. Behringer, Phys. Rev. Lett. **77**, 3110 (1996).
- [13] E. N. Bromhead, Ground Engineering **12**, 40 (1979).
- [14] C. M. Mate, M. R. Lorenz, and V. J. Novotny, J. Chem. Phys. **90**, 7550 (1989).
- [15] J. N. Israelachvili, *Intermolecular and Surface Forces*, 2nd ed. (Academic, London, 1991).
- [16] R. G. Horn, J. Am. Ceram. Soc. **73**, 1117 (1990).
- [17] R. W. Carpick, and M. Salmeron, Chem. Rev. **97**, 1163 (1997).